Long term variability of Cygnus X-1

V. State definitions with all sky monitors

V. Grinberg[1], N. Hell[1,2], K. Pottschmidt[3,4], M. Böck[5], M. A. Nowak[6], J. Rodriguez[7], A. Bodaghee[8], M. Cadolle Bel[9], G. L. Case[10], M. Hanke[1], M. Kühnel[1], S. B. Markoff[11], G. G. Pooley[12], R. E. Rothschild[13], J. A. Tomsick[8], C. A. Wilson-Hodge[14], and J. Wilms[1]

[1] Dr. Karl-Remeis-Sternwarte and Erlangen Centre for Astroparticle Physics, Friedrich Alexander Universität Erlangen-Nürnberg, Sternwartstr. 7, 96049 Bamberg, Germany
[2] Lawrence Livermore National Laboratory, 7000 East Ave., Livermore, CA 94550, USA
[3] CRESST, University of Maryland Baltimore County, 1000 Hilltop Circle, Baltimore, MD 21250, USA
[4] NASA Goddard Space Flight Center, Astrophysics Science Division, Code 661, Greenbelt, MD 20771, USA
[5] Max-Planck-Institut für Radioastronomie, Auf dem Hügel 69, 53121 Bonn, Germany
[6] MIT-CXC, NE80-6077, 77 Mass. Ave., Cambridge, MA 02139, USA
[7] Laboratoire AIM, UMR 7158, CEA/DSM - CNRS - Université Paris Diderot, IRFU/SAp, F-91191 Gif-sur-Yvette, France
[8] Space Sciences Laboratory, 7 Gauss Way, University of California, Berkeley, CA 94720-7450, USA
[9] European Space Astronomy Centre (ESA/ESAC), Science Operations Department, PO Box 78, 28691 Villañueva de la Canãda, Madrid, Spain
[10] Department of Physics, La Sierra University, Riverside, CA, USA 92515
[11] Astronomical Institute "Anton Pannekoek", University of Amsterdam, Kruislaan 403, Amsterdam, 1098 SJ, The Netherlands
[12] Astrophysics, Cavendish Laboratory, University of Cambridge, CB3 0HE, UK
[13] Center for Astrophysics and Space Sciences, University of California at San Diego, La Jolla, 9500 Gilman Drive, CA 92093-0424, USA
[14] ZP 12, NASA Marshall Space Flight Center, Huntsville, AL 35812, USA

ABSTRACT

We present a scheme to determine the spectral state of the canonical black hole Cyg X-1 using data from previous and current X-ray all sky monitors (RXTE-ASM, Swift-BAT, MAXI, and Fermi-GBM). State determinations of the hard/intermediate and soft state agree to better than 10% between different monitors, facilitating the determination of the state and its context for any observation of the source, potentially over the lifetimes of different individual monitors. A separation of the hard and the intermediate state, which strongly differ in their spectral shape and short-term timing behavior, is only possible when monitor data in the soft X-rays ($<5\,\mathrm{keV}$) are available. A statistical analysis of the states confirms the different activity patterns of the source (e.g., months to years long hard state periods or phases during which numerous transitions occurs). It also shows the hard and soft states to be stable, with the probability of Cyg X-1 remaining in a given state for at least one week to be larger than 85% for the hard state and larger than 75%, for the soft state. Intermediate states are short lived, with a probability of 50% that the source leaves the intermediate state within three days. A reliable detection of these potentially short-lived events is only possible with monitor data with a time resolution of better than 1 d.

Key words. stars: individual: Cyg X-1– X-rays: binaries – binaries: close

1. Introduction

Accreting galactic black hole binaries (BHBs) show two main spectral states: a soft state with a thermal X-ray spectrum dominated by an accretion disk and a hard state with a power law spectrum with a photon index $\Gamma \sim 1.7$. The intermediate or transitional state can be subdivided into a hard intermediate state and a soft intermediate state (Belloni 2010). Transient BHBs also show a quiescent state (McClintock & Remillard 2006). All states show distinct spectral and timing properties in the X-rays. Radio emission is detected in the hard and hard intermediate states and is strongly suppressed in the soft states (e.g., Fender et al. 2009).

In a hardness intensity diagram (HID) transient BHBs move on a clear trajectory, the so-called q-track (Fender et al. 2004). Different states correspond to different parts of the track. Of special interest is the so-called jet-line that roughly coincides with the transition from hard intermediate to soft intermediate state and is associated with radio ejection events (Fender et al. 2009). A q-track-like behavior on HIDs or on their generalization, the disk-fraction luminosity diagrams, has been found in different accreting sources such as neutron star X-ray binaries (e.g., Maitra & Bailyn 2004, Aql X-1), dwarf novae (Körding et al. 2008, SS Cyg), or AGN (Körding et al. 2006). It is therefore likely to reflect basic accretion/ejection physics inherent to a wide range of accreting objects.

Cygnus X-1 is a key source for understanding accretion and ejection processes and their connection in BHBs. It is persistent,

---

relatively nearby with a radio parallax distance of $1.86^{+0.12}_{-0.11}$ kpc (Reid et al. 2011, consistent with X-ray dust scattering halo estimates of Xiang et al. 2011), bright (above ~100 mCrab in the 1.5–12 keV band in the hard state), and often undergoes (failed) state transitions (e.g., Pottschmidt et al. 2003), which are thought to be connected to changes in its radio jet (Fender et al. 2004, 2006; Wilms et al. 2007). The black hole is in a 5.6 d orbit around its donor star, HDE 226868 (Brocksopp et al. 1999b, and references therein). The orbital modulation is also detected in radio (e.g., Pooley et al. 1999) and, due to modulation of the soft X-ray flux by absorption in the donor's stellar wind, in the X-rays (Bałucińska-Church et al. 2000; Poutanen et al. 2008). Additionally, Cyg X-1 shows a superorbital period of 150 d (Brocksopp et al. 1999a; Benlloch et al. 2004; Poutanen et al. 2008), although that superorbital variability seems to be unstable and has recently been reported to have doubled to 300 d (Zdziarski et al. 2011). In the hard state, radio jets have been observed (e.g., Stirling et al. 2001). The emisssion above ~400 keV Cyg X-1 is strongly polarized (Laurent et al. 2011; Jourdain et al. 2012).

As a persistent source Cyg X-1 does not cover the full q-track: its bolometric luminosity changes only by a factor of ~3–4 between the states (Wilms et al. 2006, and references therein) and its spectrum is never fully disk-dominated. The frequent state transitions (sometimes very fast – within hours, see, Böck et al. 2011) mean that the source often crosses the jet line. Since these state changes are thought to be associated with significant changes in the accretion flow geometry and energetics, a knowledge of the source state is crucial for the interpretation of all (multiwavelength) observations of Cyg X-1 and its donor star. A typical example is the study of the stellar wind of HDE 226868, which during soft states is strongly photoionized by the radiation from the vicinity of the black hole (Gies et al. 2008).

In the past decade, state information was readily available using the All Sky Monitor on the Rossi X-ray Timing Explorer (RXTE-ASM) and regular pointed monitoring observations. Here, various state definitions exist, which use, e.g., measured count rates and/or colors (e.g., Remillard 2005; Gies et al. 2008), or sophisticated mapping between these measurements and spectral parameters (e.g., Ibragimov et al. 2007; Zdziarski et al. 2011). The former prescription is easy to use, but is very instrument specific and cannot be translated easily to other X-ray all sky monitors. The latter approach requires a sophisticated knowledge of the instrumentation of all sky monitors as well as of the detailed spectral modeling. Furthermore, the previously used state definitions are all slightly inconsistent with each other. In this work we introduce a novel approach to classify states of Cyg X-1 using the all sky monitors RXTE-ASM, MAXI, Swift-BAT and Femi-GBM based on 16 years of pointed RXTE observations. Our aim is to find an easy-to-use prescription for the determination of states that is as consistent as possible between these instruments in order to facilitate long-term studies that exceed in duration the lifetime of individual monitors. We start with a description of our data reduction approach in Sect. 2. Section 3 comprises the actual state mapping from pointed RXTE observations to RXTE-ASM, Swift-BAT, MAXI and Fermi-GBM, including a discussion of the precision of state determinations attainable with these instruments. We summarize and discuss our results in the light of the statistics of the state behavior of Cyg X-1 in Sects. 4 and 5.

2. Observations and Data Analysis

2.1. ASM data

The RXTE-ASM instrument consisted of three Scanning Shadow Cameras (SSCs), in which a position sensitive proportional counter was illuminated through a slit mask (Levine et al. 1996). A typical source was observed at randomly distributed times 5 to 10 times a day in three energy bands roughly corresponding to 1.5–3.0 keV (band A), 3.0–5.0 keV (band B), and 5.0–12 keV (band C) (Levine et al. 1996).

We consider all 97556 RXTE All Sky Monitor (ASM, Levine et al. 1996) measurements of Cyg X-1 performed during the lifetime of RXTE. In the following all data analysis was performed with ISIS 1.6.2 (Houck & Denicola 2000; Houck 2002; Noble & Nowak 2008).

We first filter for measurements where the background was clearly oversubtracted (count rates r_A, r_B, or $r_C < 0$). The quality of the ASM data started deteriorating after about MJD 55200 (early 2010 January): valid pointings are fewer and the overall variance of the measurements becomes larger (Fig. 1). Since the larger variance could be source intrinsic, we analyze the ASM light curve of a source known to be roughly constant at the level of precision required here, the Crab (Wilson-Hodge et al. 2011): after MJD 55200 the Crab light curve shows prolonged gaps (Fig. 2). Where data exist, the average values of the ASM count rate (calculated on a 10 d timescale), which were stable at ~75 cps before, decrease by up to 10%. The variance of the data strongly increases by a factor of ~10. The ASM hardness (between the C and A bands) increases from stable values around ~0.95 up to ~1.4 and shows higher variability. The timescale of this change in behavior as well as the similar behavior of the light curves of other sources during the same time period imply that we do not see the long term variability of the Crab nebula as has been observed by Wilson-Hodge et al. (2011) here, but truly instrumental decline during the last years of the ASM lifetime.[1]

The ASM data measured post 2010 January can still be used to assess trends with large changes in count rate; for the following analysis, however, which relies on absolute values of both count rate and hardness, we ignore all ASM data after MJD 55200. Overall, we use 94068 individual ASM measurements corresponding to 80082 individual times (a source can be in the field of view of two SSCs simultaneously) spanning over 5000 days from MJD 50087 (1996 January 5) to MJD 55200 (2010 January 4).

2.2. Pointed RXTE observations

We consider all pointed RXTE observations of Cyg X-1 made during the RXTE lifetime (MJD 50071 to MJD 55931). Data from the Proportional Counter Array (PCA, Jahoda et al. 2006) and the High-Energy X-Ray Timing Experiment (HEXTE, Rothschild et al. 1998) onboard RXTE were reduced with HEASOFT 6.11 following the procedure introduced in the previous papers of this series (Pottschmidt et al. 2003; Wilms et al. 2006).

For spectral analysis of the PCA data, we use data from the top xenon layer of Proportional Counter Unit (PCU) 2 only. PCU 2 is the best calibrated PCU and had been running during all RXTE observations of Cyg X-1. We make use of the improved PCA background models and therefore only discard data within 10 minutes of the South Atlantic Anomaly (SAA; Fürst

---

[1] Vrtilek & Boroson (2013) come to similar conclusions regarding ASM data from 2010 on; they also report on gain changes in the last two years of ASM lifetime as a possible cause.
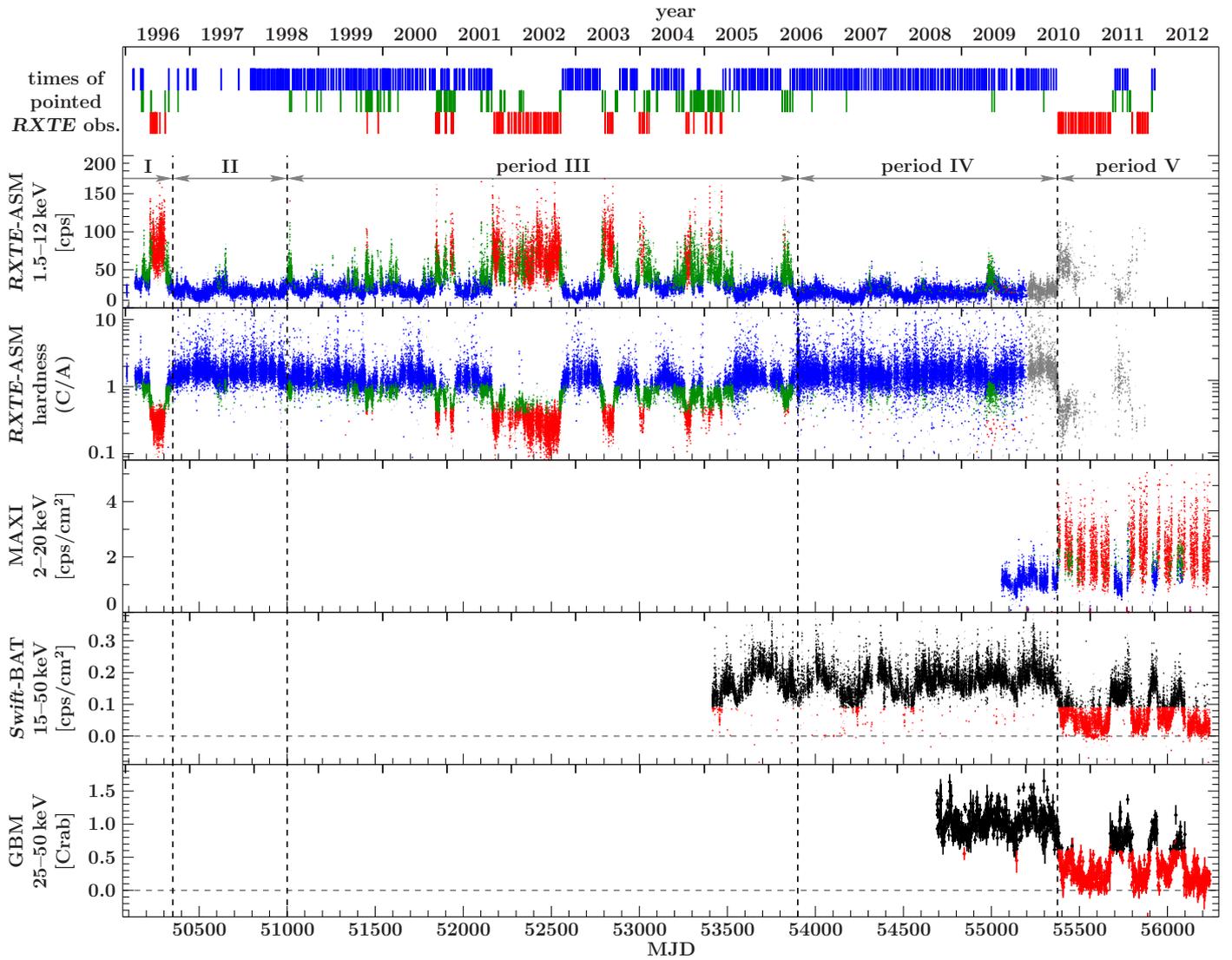
Fig. 1. Pointed RXTE observations and all light curves (RXTE-ASM, MAXI, Swift-BAT and GBM) of Cyg X-1 used in this analysis. ASM, MAXI and BAT data are shown in the highest available resolution, GBM are binned daily. ASM hardness is calculated by dividing count rates in band C (5.0–12 keV) by count rates in band A (1.5–3.0 keV). Vertical dashed lines and horizontal arrows represent periods of different source activity patterns. Blue, green, and red colors represent states of individual measurements classified using the respective classification for the different instruments as introduced in Sect. 3: blue represents the hard state, green the intermediate state and red the soft state. ASM data after MJD 55200 (shown in grey) are affected by intrumental decline. Hard and intermediate states cannot be separated in BAT and GBM; BAT and GBM data corresponding to these periods of hard or intermediate states are therefore shown shown in black.
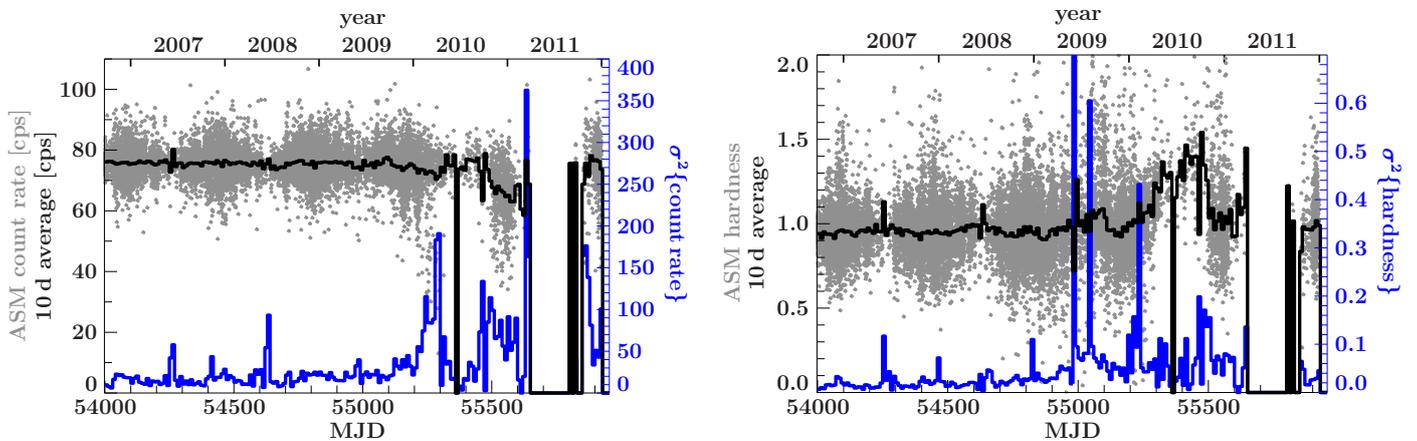

Fig. 2. Crab ASM light curve (left panel, 1.5–12 keV, gray points) and hardness (right panel, 5.0–12 keV/1.5–3.0 keV, gray points) with the respective 10 day average values (black histograms) and variances (blue histograms).

et al. 2009) passages, as opposed to the 30 minutes we used previously.

No HEXTE spectra are available during some observations either due to the non-standard observation mode employed, mainly in early observations which are not part of our bi-weekly campaign, or due to the failure of the rocking mechanism of the HEXTE clusters in the last years of the RXTE lifetime.

We extract all PCA spectra in the `standard2f` mode for each RXTE orbit and obtain 2741 individual spectra. The improved PCA background and response allow us to consider a wider energy range than previously, namely ~2.8 keV to 50 keV. The wider overlap between the PCA and HEXTE spectra, which are considered between 18 keV and 250 keV, leads to a better constraint on the multiplicative constant which accounts for the differences in the flux calibration of the two instruments. Following Böck et al. (2011) and Hanke (2011) we add a systematic error of 1% to the fourth PCA bin (2.8–3.2 keV) and of 0.5% to the fifth PCA bin (3.2–3.6 keV) in the data from PCA's calibration epoch 5 (2000 May 13 – 2012 January 5)[2], which constitute the majority of our dataset. For epochs 1 to 4 we aim for the closest possible match in energy for the systematic errors.

Where possible due to the available PCA modes, light curves with a time resolution of 2^{-9} s (~2 ms) were extracted for timing analysis, choosing the same energy bands as Böck et al. (2011): a low energy band corresponding to energies 4.5–5.7 keV (channels 11–13) and a high energy band corresponding to energies 9.4–14.8 keV (channels 23–35; energy conversion for epoch 5). The calculation of the rms and X-ray time lags follows Nowak et al. (1999). We use segments of 4096 bins, i.e., we calculate the root mean square variability (rms) between 0.125 and 256 Hz.

For two simultaneous, correlated light curves, such as the high and low energy lightcurves of Cyg X-1 used here, one can calculate a Fourier-frequency dependent time lag between the two from the Fourier phase lag at any given frequency (Nowak et al. 1999, and references therein). In our calculations a positive time lag means that the lightcurve in the hard energy band is lagging the soft. The timelag depends strongly on Fourier-frequency and shows a complex variation with state (see Pottschmidt et al. 2000, for examples and note that we use the same frequency binning in the relevant frequency-range). To obtain a single value which serves as a good signature for the overall level of the lags, we average it over the frequency range of 3.2–10 Hz (see Pottschmidt et al. 2000, 2003).

2.3. Swift-BAT, MAXI, and Fermi-GBM data

RXTE was switched off on 2012 January 5 (MJD 55931). To continue the monitoring of the long term behavior of Cyg X-1 we therefore need to use other instruments. The all sky monitor available in the soft X-ray band at the time of writing is MAXI, the hard X-rays above 10 keV are covered by Swift-BAT and the Fermi-GBM.

MAXI is an all sky monitor onboard the Japanese module of the International Space Station (Matsuoka et al. 2009). Light Curves from the Gas Slit Camera detector (GSC) are available in three energy bands (2–4 keV, 4–10 keV and 10–20 keV) on a

dedicated website[3]. MAXI light curves show prolonged gaps of several days due to observational constraints.

Swift-BAT is sensitive in the 15–150 keV regime (Barthelmy et al. 2005). Regularly updated, satellite-orbit averaged light curves in the 15–50 keV energy band from this coded mask instrument are available on a dedicated website [4].

The Gamma-ray Burst Monitor (GBM; von Kienlin et al. 2004; Meegan et al. 2007) onboard Fermi observes the sky in the hard X-ray and soft γ-ray regime (about 8 keV to ~30 MeV). It permanently provides complete coverage of the unocculted sky. Due to its strongly limited spatial resolution, the brightness of individual sources cannot be determined directly and the Earth occultation method is applied (Case et al. 2011; Wilson-Hodge et al. 2012). In this work we use the publicly available quick look Fermi GBM Earth occultation results provided by the Fermi GBM Earth occultation Guest Investigation teams at NASA/MSFC and LSU[5] which consist of light curves with a 1 d resolution in four energy bands between 12 keV and 300 keV (12–25 keV, 25–50 keV, 50-100 keV, and 100–300 keV) starting from MJD 54690. On average each measurement of Cyg X-1 is based on 18 occultations.

As these data are pre-screened by the respective instrument teams, no further selection criteria were applied and we use all data available from the start of the each mission until MJD 56240, resulting in 36454 individual measurements for BAT, 9794 for MAXI, and 1443 for GBM (Fig. 1).

3. Identifying the states of Cygnus X-1

3.1. General source behavior

The different periods of source activity and therefore the different population of the individual source states strongly affect our ability to distinguish the regions the respective states occupy on hardness-intensity diagrams (HIDs) or in other spaces. As a first step for our analysis we therefore present an overview of the light curves used for this work and over the ASM 5–12 keV to 1.5–3 keV hardness (Fig. 1).

The source behavior from early 1996 (RXTE launch) until the end of 2004 has been discussed by Wilms et al. (2006), who used a crude definition of ASM based states using the count rate only. This classification is sufficient to distinguish main activity patterns, and also consistent with more detailed studies (Zdziarski et al. 2011). We extend this earlier work and supplement the ASM data with BAT, MAXI, and GBM. By eye, i.e., without using the state definitions introduced later in this section and shown in color on Fig. 1, we are able to distinguish five main periods with different source activity patterns:

- a pronounced soft state episode in 1996 (up to ~MJD 50350, period I),
- two and a half years of a mainly stable hard state with only short softenings, seen as spiky features on Fig. 1, between the end of 1996 and early 1998 (~MJD 50350–51000, period II),
- a series of failed state transitions and soft states which started in early 1998 (Pottschmidt et al. 2003) and included a prolonged, very soft period between the end 2001 and the end of 2002. This activity period continued until mid-2006 (~MJD 51000–53900, period III),

---

- an almost continuous hard state from mid-2006 to mid-2010 which includes the hardest spectral states ever observed in Cyg X-1 (see Nowak et al. 2011, ~MJD 53900–55375, period IV),
- a series of prolonged soft states which followed an abrupt state transition at ~MJD 55375 and continued during the writing of this paper (>MJD 55375, period V).

Periods I to III are fully and period IV is almost fully covered by the ASM. Some ASM data exist during period V, but are affected by problems described in Sect. 2.1 and therefore excluded from our analysis.

During period IV the ASM hardness shows higher variability than in previous hard states, but the same effect is also seen in the hardness of the Crab and is instrumental (Fig. 2).

BAT coverage started at the end of period III on MJD 53414 (mid-February 2005) and continues during the writing of this paper. Thus, BAT data are available during soft states, namely in period V, but simultaneous coverage of soft states by BAT and ASM is lacking.

GBM and MAXI coverage started MJD 54690 (2008 August 12) and MJD 55058 (2009 August 15), respectively, and was ongoing as of time of writing. These instruments mainly cover the final phase of period IV and the ongoing period V. No simultaneous coverage with ASM exists during the intermediate and soft states, except during the phase of ASM deterioration.

During the joint coverage by ASM and BAT, Cyg X-1 displayed two softening episodes, which did not reach a stable soft state (~MJD 53800–53900 and around MJD 55000). Both episodes are clearly visible in the ASM band but not in the BAT light curve. This is a remarkable contrast to the full state transition of ~MJD 55375, which is associated with a clear drop in the BAT count rate simultaneous with an increase of ASM count rate. Similar softenings visible in the soft X-ray band but not in the hard band have been observed in 1997–1999 by Zdziarski et al. (2002), who discuss changes seen in the ASM where no corresponding changes were observed in the 20–300 keV band with BATSE. Only further long term observations in both soft and hard X-rays can help to decide whether only successful state transitions are accompanied by a change in hard X-ray flux and whether the behavior of the hard component above 15–20 keV can be used to decide whether a state transition will fail or not.

After MJD 55200 reliable ASM data are lacking. The BAT light curve suggests that while the source left the soft state for short periods of time, those hard periods were softer than the prolonged hard states in periods II and IV.

A striking feature of the hardness during the hard states are values which exceed the average by a factor of ~5 and more (Bałucińska-Church et al. 2000; Poutanen et al. 2008). They correspond to so-called X-ray dips, where blobs of cold material in the line of sight cover the source. Since it is virtually impossible to decide whether an individual ASM dwell was measured during a dip, we do not treat these data separately for the purpose of this paper (but see Boroson & Vrtilek 2010).

3.2. Γ_1 defined states

Wilms et al. (2006) have shown that the spectral shape of Cyg X-1 as observed by PCA and HEXTE (from here on: RXTE spectrum) can be well described by an empirical model which consists of a broken power law modified by a high energy cutoff, absorption described by the tbnew model, see, e.g., Hanke et al. (2009), and the abundances of Wilms et al. (2000). The iron Kα line is described by an additive Gaussian emission line

Table 1. Spearman's rank correlation coefficients ρ for the correlations between the ASM counts and the soft photon index Γ_1 of fits to pointed RXTE observations for the cases $\Gamma_1 < 2.7$ and $\Gamma_1 > 2.7$ in ASM energy bands

Energy band [keV]	1.5–12	1.5–3.0	3.0–5.0	5.0–12
ρ ($\Gamma_1 < 2.7$)	0.77	0.81	0.76	0.62
ρ ($\Gamma_1 > 2.7$)	−0.60	−0.54	−0.55	−0.68

at ~6.4 keV. The intermediate and soft states additionally show a soft excess, which is usually described by accretion disk emission (Mitsuda et al. 1984; Makishima et al. 1986). The soft photon index, Γ_1, of the broken power law shows strong correlations with other spectral and timing parameters on timescales from hours to years across the whole range of its values and is a good proxy for the source state (e.g., Pottschmidt et al. 2003; Wilms et al. 2006; Böck et al. 2011; Nowak et al. 2011).

We model all spectra both with and without a disk and accept the disk as real if the addition of the disk component improves the χ^2 value by more than 5%[6]. With this approach, we are able to achieve good fits ($\chi^2_{red} < 1.2$) for almost all spectra, with a few outliers not exceeding $\chi^2_{red} = 2.5$. Less than 18% of the spectra with $\Gamma_1 < 2.0$ require a disk, but 97% of the fits with $\Gamma_1 > 2.0$ do. This agrees with the known behavior of the disk in black hole binaries in the different states (e.g., Belloni 2010). For all best fit models, we obtain $\Gamma_1 > \Gamma_2$ and $E_{break} \sim 10$ keV. For a more detailed discussion of the fits to then available data and examples of typical spectra we refer to Wilms et al. (2006).

Figure 3 shows the dependence of the total rms between 0.125 and 256 Hz in both high and low energy bands and the time lag (averaged between 3.2 and 10 Hz) on the soft photon index Γ_1. The timing and spectral behavior is clearly related, but complex with changes in both slope and sign. For clarity of the plot we do not show error bars; the uncertainty of single measurements is, however, on the order of or smaller (in the case of the hard observations: much smaller) than the spread of the correlation at any given frequency. $\Gamma_1 \sim 2$, where spectral models with a disk become dominant, corresponds to a bend in the timing correlations. Another clear kink can be seen at $\Gamma_1 \sim 2.5$.

We use both our spectral and timing analysis results to define Γ_1 ranges for different source states that are characterized by spectral and timing behavior which is similar within a state but different between the three states. Hard states correspond to $\Gamma_1 < 2.0$, intermediate states correspond to $2.0 < \Gamma_1 < 2.5$, and soft states correspond to $\Gamma_1 > 2.5$.

3.3. Simultaneous ASM mapping

For direct classification of the ASM data we use the 1424 instances when ASM observations of Cyg X-1 are simultaneous with spectra from pointed RXTE observations, i.e., fall within the good time intervals used for the orbit-wise spectral extractions. This corresponds to 2400 individual ASM measurements since the source is often observed by more than one SSC. We treat the measurements of different SSCs independently for the actual mapping since instrument alignment onboard RXTE would otherwise introduce a bias towards a higher number of ASM measurements with Cyg X-1 in the field of view of two SSCs during pointed observations of Cyg X-1.

---

[6] Since the PCA data in the lower channels are dominated by systematic errors for a source as bright as Cyg X-1, it is not possible to adopt a significance-based criterion for the improvement in χ^2.
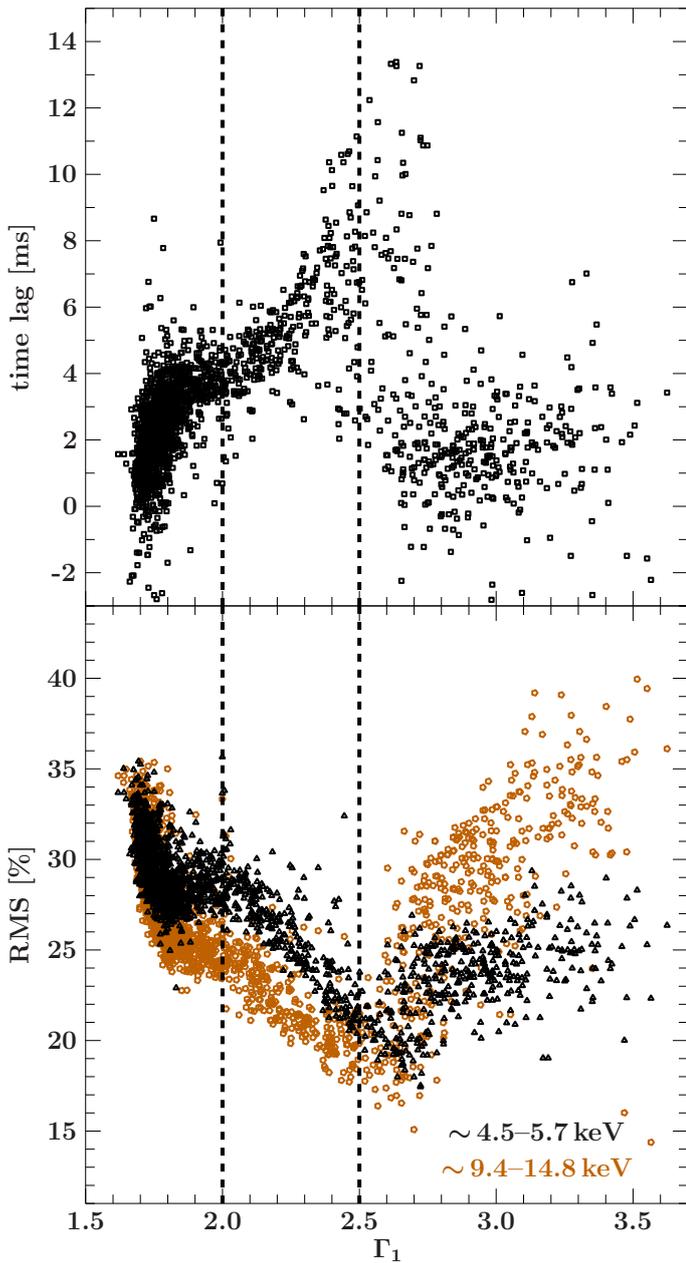
Fig. 3. X-ray time lag and fractional RMS as a function of the soft photon index Γ_1.

Figure 4 shows the dependence of the ASM count rate from individual ASM-SSC dwells on the soft photon index Γ_1 of the broken power law fits. Note that due to the use of individual ASM SSC dwells, an RXTE spectrum and therefore a Γ_1-value can correspond to more than one simultaneous ASM measurement. While the ASM count rate in all bands is correlated with Γ_1, this correlation is not unique: it appears to change sign at $\Gamma_1 \sim 2.7$ (Table 1). Consistent with this observation, Zdziarski et al. (2011) note that on several instances in the soft state their derived bolometric flux is lower than during the high-flux hard state[7]. Thus, cuts in ASM count rate alone cannot separate the states.

---

[7] Zdziarski et al. (2011) define the soft state according to a power-law photon index deduced from the ASM count rates. This approach does not exactly correspond to the approach chosen here, however, it is similar enough to allow rough comparisons.
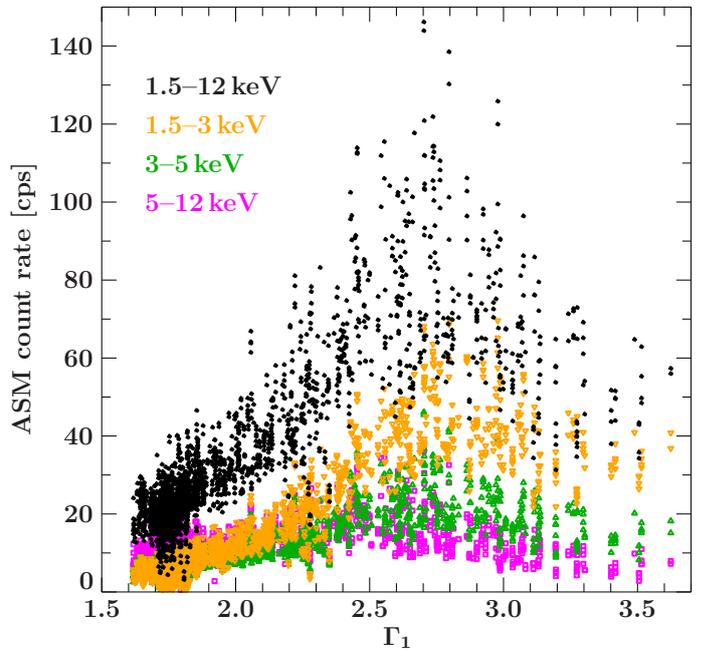
Fig. 4. Dependence of the ASM count rate in different bands on the soft photon index Γ_1 of simultaneous pointed RXTE observations. Shown are total ASM counts (1.5–12 keV, black dots) and counts in the three ASM energy bands: band A (1.5–3 keV, orange upside down triangles), band B (3–5 keV, green triangles) and band C (5–12 keV, magenta squares).

The Γ_1-based definition of states introduced in Sect. 3.2 results in in 1608 ASM measurements in the Γ_1-defined hard state, in 455 ASM measurements in the Γ_1-defined intermediate state, and in 337 ASM measurements in the Γ_1-defined soft state. Each of the states primarily populates a well-defined distinct area in the ASM HID (Fig. 5). A visual inspection reveals that neither cuts in hardness only nor cuts in count rate only yield a good division between the states: the softest observations tend to have count rates in the transitional state range ($\sim$40–50 cps), the hard state area extends to low hardnesses usually associated with transitional or even soft states, and the hard and transitional state strongly overlap both in ASM hardness and count rate. To account for these features we choose the following ansatz: an ASM observation with count rate c and (5–12 keV/1.5–3 keV) hardness h is defined as hard if $c \leqq 20$ cps regardless of the hardness. For $c > 20$ cps the cuts between the states are defined by linear functions of the form

$$c_{\mathrm{ASM}} = m_{\mathrm{ASM},i} \cdot (h - h_{0,i}) \qquad (1)$$

where $i \in \{\mathrm{hard}, \mathrm{soft}\}$. The line with slope $m_{\mathrm{ASM,hard}}$ and x-intersection $h_{0,\mathrm{hard}}$ divides the hard and the intermediate state, and the line with slope m_{soft} and intersection $h_{0,\mathrm{soft}}$ divides the intermediate and the soft state, respectively.

We determine the best division between the states such that the fractional contamination of the ASM-defined states by different Γ_1-defined states is minimized. Contamination here is defined for the hard state (and accordingly for soft and transitional states) as the fraction of all measurements classified as hard using the ASM that is classified as transitional or soft according to Γ_1. Initial fits indicate that good separations of the states are achieved for $h_{0,\mathrm{hard}} \sim h_{0,\mathrm{soft}}$. We therefore reduce the number of free parameters for the cuts and set

$$h_{0,\mathrm{hard}} = h_{0,\mathrm{soft}} = h_0. \qquad (2)$$

Table 2. Overview over all sky monitor based state definitions for Cyg X-1.

State	ASM-based[a]	MAXI-based[b]	BAT-based[c]	GBM-based[d]
hard	$c \leq 20 \vee c \leq 55 \cdot (h - h_0)$	$c_M \leq 1.4 \cdot h_M$	$\ldots$[e]	$\ldots$[f]
interm.	$c > 20 \wedge 55 \cdot (h - h_0) < c \leq 350 \cdot (h - h_0)$	$1.4 \cdot h_M < c_M \leq 8/3 \cdot h_M$	$\ldots$[e]	$\ldots$[f]
soft	$c > 20 \wedge c > 350 \cdot (h - h_0)$	$8/3 \cdot h_M < c_M$	$c_B \leq 0.09$ counts cm^{-2} s^{-1}	$f \leq 0.6$ Crab

Notes. [a] With ASM 1.5–12 keV count rate c in counts s^{-1}, ASM (5–12 keV/1.5–3 keV) hardness h, and $h_0 = 0.28$. [b] With MAXI 2–4 keV count rate c_M in counts s^{-1} and MAXI (4–10 keV/2–4 keV) hardness h_M. [c] With BAT normalized 15–50 keV countrate c_B in counts cm^{-2} s^{-1}. [d] With daily GBM 25–50 keV flux f. [e] Discriminating between hard and intermediate states is not possible based on BAT lightcurves alone. The source is defined as in BAT-based hard *or* intermediate state for $c_B > 0.09$ counts cm^{-2} s^{-1}. [f] Discriminating between hard and intermediate states is not possible based on GBM daily lightcurves alone. The source is defined as in GBM-based hard *or* intermediate state for $f > 0.6$ Crab.
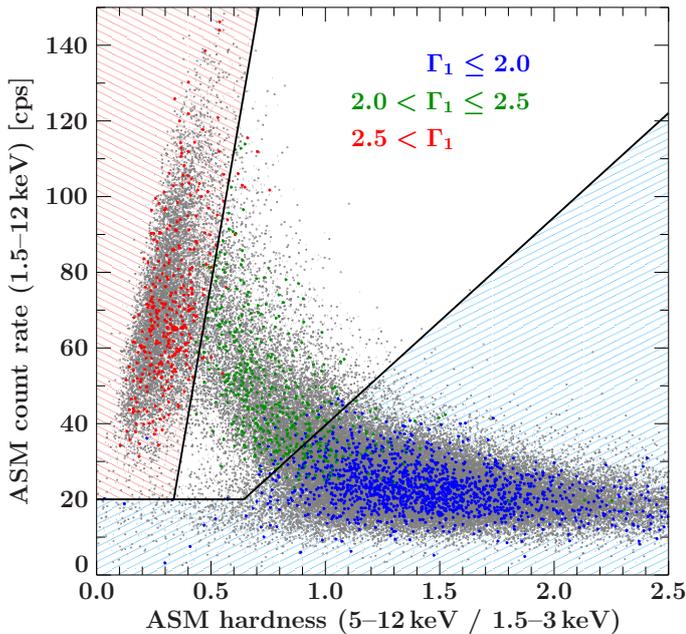

Fig. 5. PCA to ASM mapping. Grey data points are all ASM measurements of Cyg X-1 in the shown range. Blue points represent PCA defined hard states, green intermediate and red soft states. Black lines show the cuts defining the states in the ASM HID. The light blue shaded region corresponds to the position of the hard state in the HID, the light red shaded to the position of the soft state. The intermediate state region is shown without shading.

Fig. 6. Percentage of contamination of the ASM defined states (hard state shown in blue, intermediate in green, and soft in red) for time delays $\Delta t = \pm(0$–$1.5)$ h, $\pm(1.5$–$3)$ h, $\pm(3$–$4.5)$ h, etc., between the ASM and the pointed RXTE measurements. Simple linear fits to the data are shown as dashed lines to illustrate the overall trends.

For the best cuts we obtain $h_0 = 0.28$, $m_{\text{hard}} = 55$, and $m_{\text{soft}} = 350$ (Fig. 5 and Table 2).

The contamination by other Γ_1-defined states is <5% for the hard state, <10% for the intermediate state and <3% for the soft state. Note that since the source behavior changes continuously from one state to the other, such that the states do not represent three distinct, fully independent regimes, we do not expect a perfect separation of the states (e.g., Wilms et al. 2006). The spread in count rate and hardness is amplified by the orbital and super-orbital modulations of Cyg X-1 and by dips (e.g., Poutanen et al. 2008). The stronger contamination of the intermediate state is expected: as a transitional state between the hard and the soft state, it is short-lived and confined by two divisional lines. The separation between the hard and the intermediate state appears especially unclean; we therefore advise to treat the classification cautiously when an observation is close to this cut.

To test our approach we compare the ASM-based behaviour with the results of the spectro-timing analysis of the quick, observationally exceptionally well covered intermediate to soft transition presented by Böck et al. (2011). In particular, we
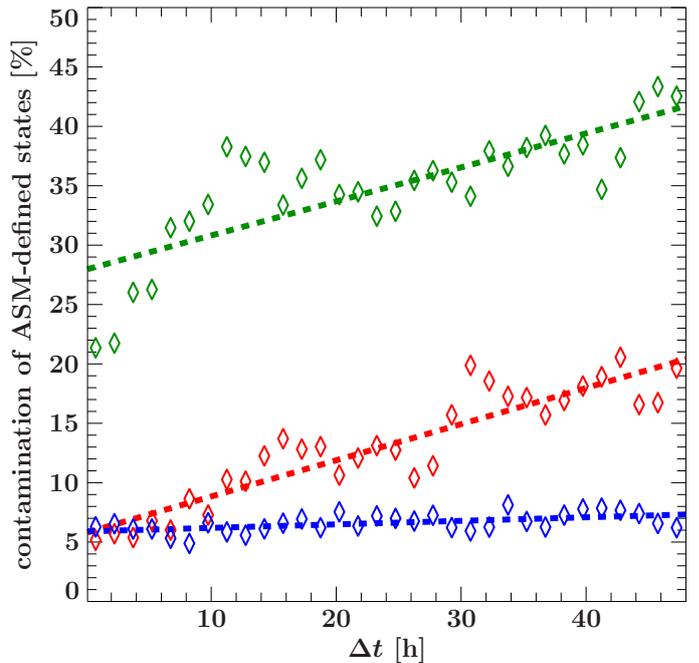
can recover the moment of the transitions at slightly before MJD 53410.

3.4. Non-simultaneous ASM mapping

In general, an all sky monitor and a pointed instrument will not observe a source at the same time, so that we need to assess how well a given monitor pointing can be used to characterize the source state during a non-simultaneous observation.

For every RXTE spectrum we consider ASM measurements within 1.5 h intervals $\Delta t = \pm(0$–$1.5)$ h, $\pm(1.5$–$3)$ h, $\pm(3$–$4.5)$ h, etc., up to 48 hours. The length of the intervals is motivated by the length of the RXTE orbit of ~1.5 h, during about half of which Cyg X-1 is visible. For simultaneous ASM measurements with different SSCs we use the average for all following analysis. We obtain 135901 pairs of ASM and RXTE state classifications (the same ASM measurement may be used to classify several RXTE spectra, if the RXTE spectra are close enough). For every delay interval and for every ASM defined state, we determine the percentage of spectra with a different RXTE classification.
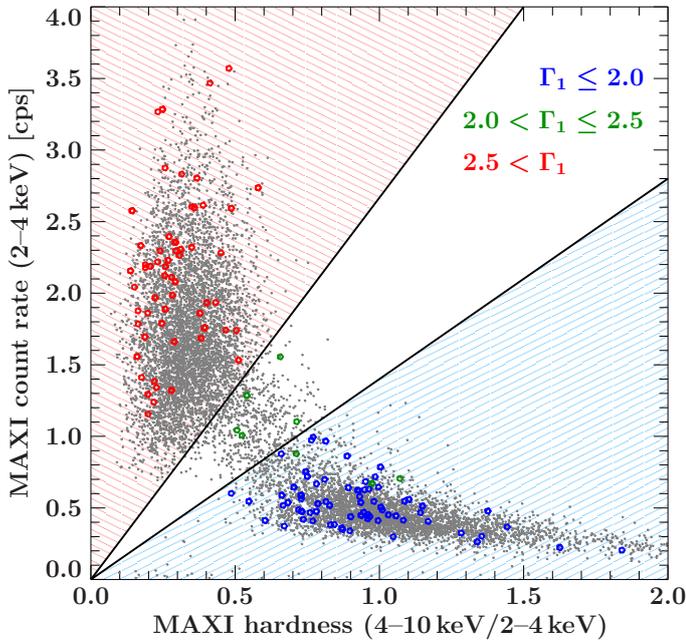
Fig. 7. PCA to MAXI mapping. Gray data points are all MAXI orbitwise measurements of Cyg X-1 in the shown energy range. Blue circles represent PCA defined hard states, green intermediate states and red soft states. Black lines define the state cuts. The light blue shaded region corresponds to the hard state in the MAXI HID, the light red shaded region to the soft state and the region without shading to the intermediate state.

Figure 6 shows that this contamination remains stable for the hard state for up to ∼48 h. For the soft state, the contamination reaches 20% for a 48 h delay and is even larger for the intermediate state, which also shows a very strong increase within the first ∼10 h. Note that strictly simultaneous data, which were discussed in Sect. 3.3, are not taken into account here, resulting in larger starting contaminations. The results are similar when using positive or negative delays only. The trends are expected, because the hard state occurred often in long, stable stretches during the RXTE lifetime, while the intermediate state is short lived due to its transitional nature.

3.5. MAXI mapping

Since only 37 MAXI measurements are strictly simultaneous with pointed RXTE data, we use MAXI data within $\Delta t = 1$ h before and after a pointed RXTE observation and obtain 219 MAXI measurements with Γ_1-based state classifications, which offer a better overall statistics with 107 hard states, 101 soft states, and 11 intermediate states. Increasing Δt to 2 h does not yield a better coverage of the intermediate state, neither does attempting to map ASM onto MAXI, since a simultaneous coverage by the two instruments is only available during the end of period IV.

To find the best approach to define MAXI based states we consider all possible different combinations of count rates measured with MAXI (the three energy bands as introduced in Sect. 2.3 and the overall count rate) and different combinations of hardness measures within the MAXI bands. The clearest separation can be achieved when using the ratio between count rates in the medium (4–10 keV) and the low (2–4 keV) MAXI bands (MAXI-hardness, h_{MAXI}) and the count rate in the low (2–4 keV) MAXI band, c_{MAXI}, as done in Fig. 7. The MAXI 4–10 keV/2–
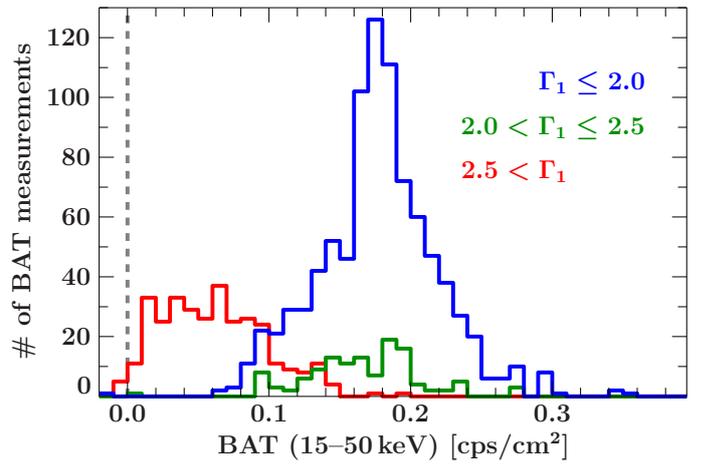
Fig. 8. Histogram of BAT fluxes of Γ_1-defined states: the hard state is shown in blue, the intermediate state in green, and the soft state in red.

4 keV hardness is also the closest correspondence to ASM hardness we can achieve using publicly available MAXI light curves.

The sparse coverage of the intermediate state makes it hard to separate the three basic states. Given that the hard and the soft state populate distinct parts of the MAXI HID (see Fig. 7) and knowing the shape of the cuts in the ASM HID, we separate the states by two linear functions of the form

$$c_{\text{MAXI}} = m_{\text{MAXI},i} \cdot h_{\text{MAXI}}, \qquad (3)$$

where $i \in \{\text{hard}, \text{soft}\}$ and where m_{hard} separates the hard and the intermediate state and m_{soft} separates the intermediate and the soft state. The absence of an x-intersection and of a threshold count rate value is motivated by the lower number of classified data points compared to the ASM HID, which also prevents us from direct fits for m. The best values obtained by eye are $m_{\text{MAXI,hard}} = 1.4$ and $m_{\text{MAXI,soft}} = 8/3$ (Table 2).

For a reader interested in performing her own classification using MAXI data, we note that these are conservative cuts in the sense that we obtain the purest intermediate state possible here. As in the case of RXTE-ASM we expect the separation between the hard and intermediate state to be especially unclean.

3.6. BAT mapping

Swift-BAT light curves in different energy bands are not readily available. Since BAT also does not cover soft X-ray energies where the contribution of the accretion disk becomes important as the spectrum softens, we use only the light curves in the standard 15–50 keV band for our analysis and therefore do not perform a two-dimensional mapping.

Since only 290 BAT measurements are strictly simultaneous with pointed RXTE data, we employ the same approach as for MAXI (Sect. 3.5) and use BAT data within $\Delta t = 1$ h before and after the RXTE spectrum to obtain 1339 BAT measurements with an RXTE based state classification: 895 in the hard state, 124 in the intermediate state, and 320 in the soft state.

Only 290 BAT measurements are strictly simultaneous with pointed RXTE data. Following our study of the reliability of non-simultaneous data (Sect. 3.4), we use BAT data within $\Delta t = 1$ h before and after a pointed RXTE observation and obtain 1339 BAT measurements with Γ_1-based state classifications, which offer a better overall statistic.

Figure 8 shows the histogram of the BAT fluxes in the different states. While the soft and hard state show clearly different

BAT fluxes, the intermediate states populate the same region as the hard ones. The BAT measurements, therefore, do not enable us to separate the hard and the intermediate states. The soft state can still be identified by a cut at a BAT area normalized count rate of $c_{BAT} = 0.09\,\mathrm{counts\,cm^{-2}\,s^{-1}}$ For BAT count rates below c_{BAT} Cyg X-1 is in the soft state, for fluxes above it in the hard or intermediate state (Table 2). The contamination by the other state is ~7% in both cases.

We also considered an ASM to BAT mapping where we classified BAT data by using the closest ASM measurements if one exists within ±0.5 h around the BAT measurement in order to increase the number of data points with classification. No simultaneous good ASM and BAT data are available in the soft state (see Fig. 1 and Sect. 2.1). The histograms of the hard and intermediate state follow the trends apparent from Fig. 8: it is not possible to separate the two states using BAT flux.

3.7. GBM mapping

Since GBM lightcurves are publicly available in daily bins only, strictly simultaneous mapping between RXTE spectra and GBM is not possible. We therefore define an RXTE spectrum as simultaneous to a GBM measurement if the good time interval used to extract the spectrum lies within the GBM measurement. If all simultaneous RXTE spectra show the same state, the GBM measurement is classified as belonging to this state. If the states of the RXTE spectra differ, the GBM measurement is not classified.

The 104 GBM measurements with simultaneous RXTE observations include on average 3.8 (reaching from 1 to 8) individual RXTE spectra. Only 6 out of the 104 measurements are unclassified due to state ambiguities. The remaining valid classifications include 61 hard states, 3 intermediate states, and 34 soft states. All 6 unclassified measurements include hard as well as intermediate state classifications. There were no GBM measurements including both intermediate and soft, or hard and soft RXTE spectra. The distribution of these results is consistent with Cyg X-1 spending most of the time covered by GBM observations in stable hard and soft states. That 6 out of 9 GBM measurements including a Γ_1-defined intermediate state also include Γ_1-defined hard states reflects the high variability and instability of the intermediate states.

We first consider GBM HIDs. These show a clear separation in two regions: a region with mainly soft and a region with hard and intermediate observations, which are clearly separated in GBM flux only. We therefore consider GBM fluxes only and calculate histograms of GBM fluxes of Γ_1-defined states. The best separation between the states can be achieved when using 25–50 keV fluxes (Fig. 9). While hard and intermediate states cannot be separated, the soft state can be divided from the other two by a cut at a GBM flux of 0.6 Crab: for fluxes <0.6 Crab the source is in the soft state, for fluxes ≥0.6 Crab in hard or intermediate state (Table 2). We do not give values for contamination here because of the long integration times of the GBM and because we excluded states where we know the source to change the Γ_1 defined state during one GBM measurement. We also note, that since the hard and intermediate states cannot be distinguished using GBM, we do not introduce additional bias into our classification by not including GBM-measurements with simultaneous RXTE spectra in both hard and intermediate states.

4. The states of Cyg X-1

4.1. The statistics of Cyg X-1 states

Using the classification from the different instruments derived in the previous sections, we can assess the activity pattern during the different periods defined in Sect. 3.1. A detailed break-down of the occurence of different states is given in Table 3.

Period ı contained a prolonged soft state and the source spent twice as much time in soft states than in the intermediate state during this time. We lack all sky monitor coverage before MJD 50087 and therefore do not know whether this soft period observed was a part of a longer series of soft states.

In period ııı the source spent as much time in the intermediate state as in the soft state, in accordance with the observation of multiple failed state transitions (e.g., Pottschmidt et al. 2003).

Periods ıı and ıv showed similar activity patterns dominated by a long, stable hard state, although data from the ASM were already affected by deterioration of the instrument in period ıv (Sect. 3.1). The state classifications based on the ASM and the BAT agree well for period ıv.

The disagreement between the statistics derived from Swift-BAT and MAXI classification for period v first seems worrisome. A visual inspection of Fig. 1 indicates, however, that this mismatch may be due to the gaps in the MAXI light curve. Indeed, out of the 7794 BAT measurements which fall into MAXI gaps (defined here as times when the interval between two MAXI measurements is larger than 6 h), 3876 are hard or intermediate and 3918 are soft, while 60% of all BAT measurements during period v are soft. MAXI gaps therefore fall more often onto hard/intermediate states than onto soft states during this period and the difference seen in Table 3 is due to the incomplete MAXI coverage. MAXI data can therefore be used to determine states at certain times, but not to investigate the overall frequency of the occurrence of different states. A similar caution also applies to the GBM. Here, the disagreement between the GBM data and other instruments is partly due to the use of daily lightcurves, where the short term variability is averaged out (Fig. 1). This can be directly seen from the higher resolution BAT data. Using individual BAT points during period v, 60% of all measurements are classified as coming from the soft state (Table 3). Classifying the daily BAT fluxes, however, increases the fraction of soft states to 68%, which is consistent with the GBM considering the uncertainties in both the GBM- and BAT-based definitions (Figs. 8 and 9). Data with a time resolution <1 d are therefore crucial for a reliable state classification.

Summarizing these observations, we estimate the typical inter-instrument systematic error of the state determination to be better than 10% for the post-RXTE instruments.

4.2. Stability of States

Sect. 4.1 highlights that the different states are clearly different in their stability. While the source tends to remain in the hard and the soft state for a prolonged time, not unexpectedly the intermediate state is far more unstable. This well known general behavior can be quantified using the RXTE-ASM data, the data set in our measurements that covers the longest time span, does not have gaps, and can be reliably used to define all three states.

To calculate the state statistics, for each ASM data point measured at a reference time, t_{ref}, we calculate the probability that Cyg X-1 has changed its state after a certain interval, and the probability that the source remained in the same state throughout this interval. More formally, we calculate the transited fraction,
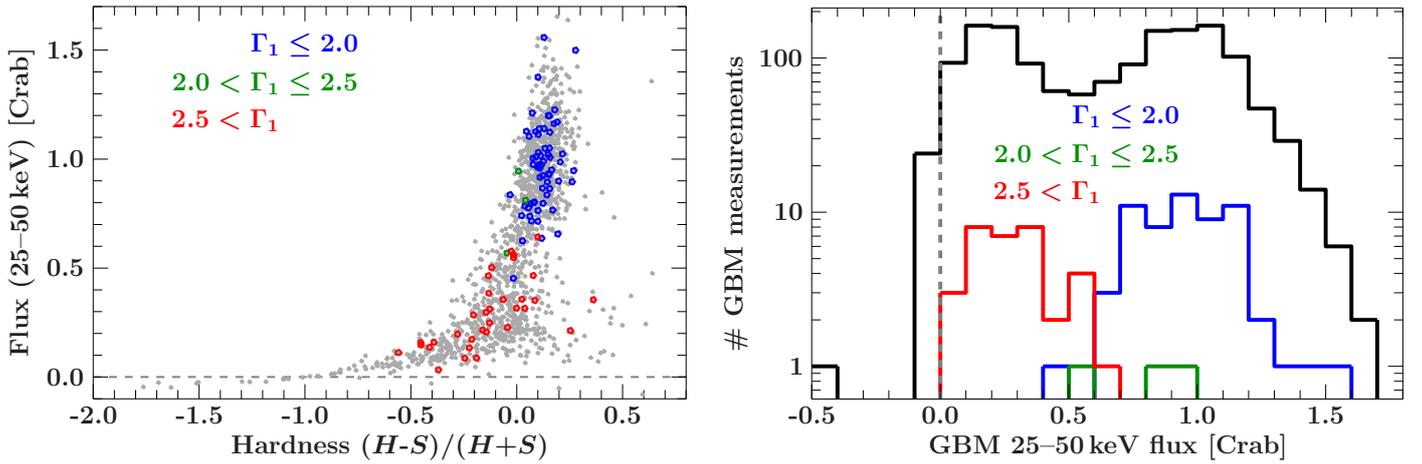
Fig. 9. *Left:* Daily GBM HID. *S* denotes the 12–25 keV flux, *H* the 25–50 keV flux. The gray dashed line denotes the zero flux level. Total GBM measurements are shown in gray. *Right:* Histogram of daily GBM fluxes of Γ_1-defined states. The hard state is shown in blue, intermediate state in green, and soft state in red. Total GBM measurement are shown in black. The gray dashed line denotes the zero flux level.

Table 3. Time Cyg X-1 spent in the different states (hard – H, intermediate – I, soft – S) as measured by the RXTE-ASM, Swift-BAT, MAXI and Fermi-GBM all sky monitors.

Period[a]	MJD	RXTE-ASM			MAXI			Swift-BAT		Fermi-GBM	
		H	I	S	H	I	S	H & I	S	H & I	S
I	50087[b]–50350	37%	19%	44%	...	...	...	...	...	...	...
II	50350–51000	99%	1.0%	0%	...	...	...	...	...	...	...
III	51000–53900	63%	20%	17%	...	...	...	...	...	...	...
IV	53900–55375	97%[d]	2%[d]	<1%[d]	...	...	...	99%	1%	...	...
V	55375–56240[c]	...	...	...	17%[e]	8%[e]	75%[e]	40%	60%	23%[f]	77%[f]

Notes. Between MJD 50087 and 55200 Cyg X-1 spent a total of 75.6% of its time in the hard state, 12.8% in the intermediate state and 11.6% in the soft state as measured with ASM.
Percentages are only shown if at least most of the period is covered by the respective instrument. [a] Periods defined in Sect. 3.1. [b] Start of period I defined by the start of the RXTE-ASM measurements. [c] The end of period V is defined by the availability of data at the time of writing. [d] ASM data only until MJD 55200. [e] MAXI data affected by gaps in the lightcurve. [f] Daily average values are used for GBM.

P_{trans}, i.e., the probability that an observation made a certain time *after* the reference observation will find Cyg X-1 in a different source state (Fig. 10). The probability that the source state is unchanged is $1 - P_{\text{trans}}$. We determine P_{trans} by calculating the fraction of all measurements in a different state than the reference measurement made at times t_i with $\Delta t_1 \leq t_i - t_{\text{ref}} < \Delta t_2$ where $\{\Delta t_1, \Delta t_2\} \in \{\{0\,\text{h}, 1.5\,\text{h}\}, \{1.5\,\text{h}, 3.0\,\text{h}\}, \{3.0\,\text{h}, 4.5\,\text{h}\}, \ldots\}$. This approach is equivalent to that employed in Sect. 3.4, where we used RXTE spectra as reference measurements.

P_{trans} does not take into account the possibility that the source might have undergone state changes between t_{ref} and t_i. To address this possibility we calculate the cumulative transited fraction, $P_{\text{ct},n}$, which measures the probability that at least one source transition has happened up to a time interval Δt after the reference measurement. In order to assess the influence of possible outliers and/or misclassifications, we define a state transition by the existence of more than $n \in \{0, \ldots, 12\}$ measurements in a different state than the reference measurement in the time interval $t_{\text{ref}} \leq t < t_{\text{ref}} + \Delta t$. The probability that the source has remained in the same state for at least a time Δt is then given by $1 - P_{\text{ct},n}$ (Fig. 11).

As expected from a simple look at the lightcurves (see Fig. 1) hard states are the most stable states: in more than 90% of all cases, 200 h after a given hard state ASM measurement the source is still in the hard state (Fig. 10). In over 30% of all cases a period of 300 h after any given hard state measurement will

not contain even a single measurement in a different state. This number increases to over 70% for larger n, i.e., when very short excursions to the soft/intermediate state and/or outliers due to misclassifications are ignored (Fig. 11).

Though less stable and shorter than hard states, soft states generally show a similar behavior. Even for $n = 0$, a significant number of soft state measurements is not followed by a state transition within 300 h, i.e., prolonged stable, soft states lasting more than 12 days exist. Such states are observed by ASM in periods I and III (Fig. 1). MAXI and BAT data suggest an increased occurrence of such stable soft states also in period V.

The intermediate state behaves differently. The transited fraction strongly increases within the first few hours. Already fifty hours after a reference intermediate measurement about half of the measurement will show the source in a different state. The cumulative transited fraction approaches 100% even for $n = 12$ at 300 d (Fig. 11). Intermediate states are therefore short and unstable compared to hard and soft states.

5. Summary

Based on pointed RXTE observations, we provided criteria to define X-ray states (hard, intermediate, and soft) using light curves from all sky monitor instruments. In particular we have shown that:
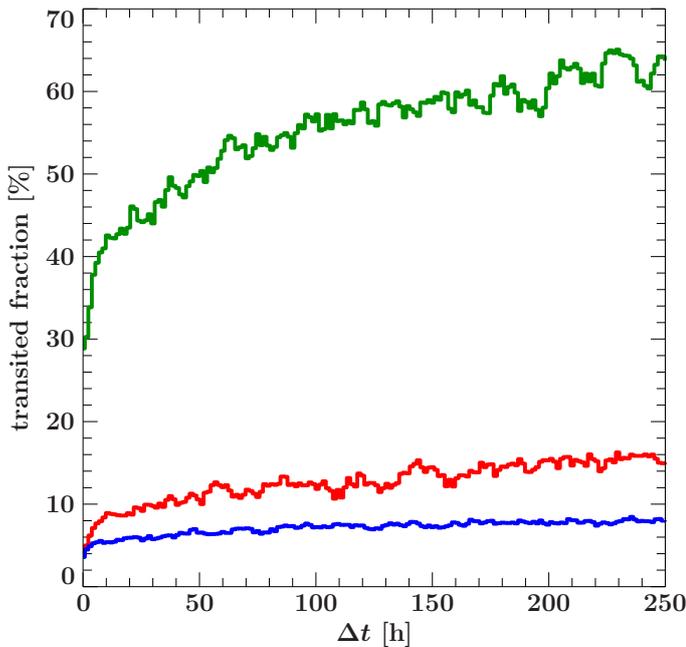
Fig. 10. Probability, P_{trans}, that the source state is found changed a time interval Δt after a previous state determination for the different states (blue: hard, green: intermediate, red: soft) using ASM data.
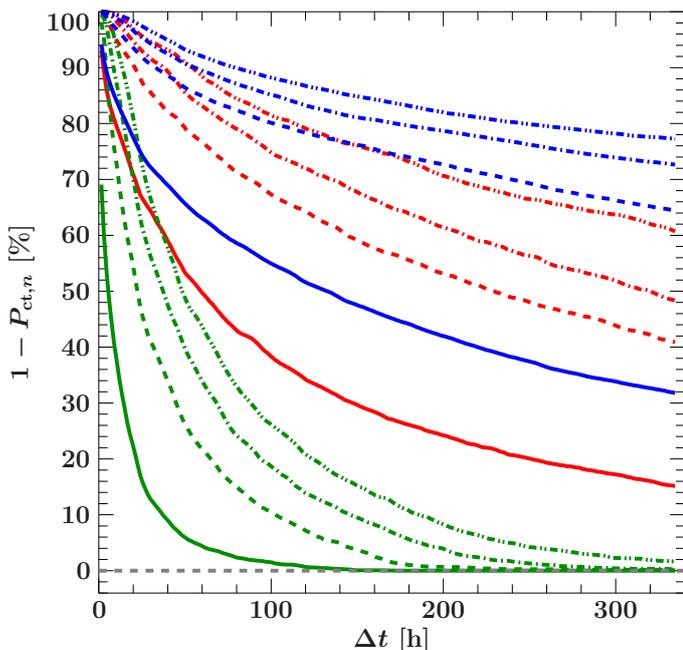

Fig. 11. The probability, $1 - P_{\text{ct},n}$, that the source has remained in the same state (blue: hard, green: intermediate, red: soft) for at least the time Δt for different values of n of ignored number of possible outliers/misclassifications ($n = 0$: solid, $n = 4$: dashed, $n = 8$: dot-dashed, $n = 12$: dot-dot-dashed). The gray dashed line represents 0.

– due to the complex source behavior, simple state definitions based just on the source count rate or just on the hardness do not adequately describe states,

– a combination of RXTE-ASM total count rate and hardness can be used to define states before MJD 55200 (see Table 2 for exact cut),

– the best separation of states is achieved with simultaneous ASM data. Data within $\Delta t \pm 6\,\text{h}$ result in a contamination of

<10% for the hard and soft state and <30% for the intermediate state,

– a combination of MAXI count rate and hardness can be used to define states (see Table 2 for exact cuts),

– soft coverage is necessary to define states and the lack of such does not allow to distinguish the hard and the intermediate state using publicly available BAT light curves. BAT light curves can, however, be used to distinguish the soft state from hard/intermediate states: the source is in the soft state below a threshold of $0.09\,\text{counts}\,\text{cm}^{-2}\,\text{s}^{-1}$, and in the hard/intermediate state above it (Table 2),

– the lack of soft coverage does not allow a separation between hard and intermediate state with publicly available GBM data, with the analysis being further hindered by the low time resolution of the GBM lightcurve, but a rough state classification is to consider Cyg X-1 in the soft state for fluxes <0.6 Crab and in the hard/intermediate state above that threshold (Table 2),

– the hard state is by far the most stable state of Cyg X-1, followed by the soft state. The probability that the source remains in the hard state for at least one week (200 h) is >85% (using $P_{\text{ct},12}$). Soft states are slightly less stable, but the probability of a soft state being longer than one week is still ~75%. Intermediate states are short-lived and typically last a few days at most, implying that they can only be caught with monitor data with a time resolution of better than 1 d.

The state classification introduced here can be reliably used to define source states where no X-ray continuum spectrum measurement is available. The high frequency of all sky monitor measurements for RXTE-ASM, Swift-BAT, and MAXI enables us to catch short flares and especially quick state transitions.

References

Bałucińska-Church M., Church M.J., Charles P.A., et al., 2000, MNRAS 311, 861

Barthelmy S.D., Barbier L.M., Cummings J.R., et al., 2005, Space Sci. Rev.120, 143

Belloni T.M., 2010, In: T. Belloni (ed.) Lecture Notes in Physics, Berlin Springer Verlag, Vol. 794. Lecture Notes in Physics, Berlin Springer Verlag, p. 53

Benlloch S., Pottschmidt K., Wilms J., et al., 2004, In: Kaaret P., Lamb F.K., Swank J.H. (eds.) X-ray Timing 2003: Rossi and Beyond. AIP Conf. Ser. 714, p.61

Böck M., Grinberg V., Pottschmidt K., et al., 2011, A&A 533, A8

Boroson B., Vrtilek S.D., 2010, ApJ 710, 197

Brocksopp C., Fender R.P., Larionov V., et al., 1999a, MNRAS 309, 1063

Brocksopp C., Tarasov A.E., Lyuty V.M., Roche P., 1999b, A&A 343, 861

Case G.L., Cherry M.L., Wilson-Hodge C.A., et al. 2011, ApJ 729, 105

Fender R.P., Belloni T.M., Gallo E., 2004, MNRAS 355, 1105

Fender R.P., Homan J., Belloni T.M., 2009, MNRAS 396, 1370

Fender R.P., Stirling A.M., Spencer R.E., et al., 2006, MNRAS 369, 603

Fürst F., Wilms J., Rothschild R.E., et al., 2009, Earth and Planetary Science Letters 281, 125

Gies D.R., Bolton C.T., Blake R.M., et al., 2008, ApJ 678, 1237

Hanke M., 2011, Ph.D. thesis, Universität Erlangen-Nürnberg

Hanke M., Wilms J., Nowak M.A., et al., 2009, ApJ 690, 330

Houck J.C., 2002, In: G. Branduardi-Raymont (ed.) High Resolution X-ray Spectroscopy with XMM-Newton and Chandra., published electronically

Houck J.C., Denicola L.A., 2000, In: Manset N., Veillet C., Crabtree D. (eds.) Astronomical Data Analysis Software and Systems IX. ASP Conf. Ser. 216, p. 591

Ibragimov A., Zdziarski A.A., Poutanen J., 2007, MNRAS 381, 723

Jahoda K., Markwardt C.B., Radeva Y., et al., 2006, ApJS 163, 401

Jourdain E., Roques J.P., Chauvin M., Clark D.J., 2012, ApJ761, 27

Körding E., Rupen M., Knigge C., et al., 2008, Science 320, 1318

Körding E.G., Jester S., Fender R., 2006, MNRAS 372, 1366

Laurent P., Rodriguez J., Wilms J., et al., 2011, Science 332, 438

Levine A.M., Bradt H., Cui W., et al., 1996, ApJ 469, L33

Maitra D., Bailyn C.D., 2004, ApJ 608, 444

Makishima K., Maejima Y., Mitsuda K., et al., 1986, ApJ 308, 635

Matsuoka M., Kawasaki K., Ueno S., et al., 2009, PASJ61, 999

McClintock J.E., Remillard R.A., 2006, In: Compact Stellar X-ray Sources., Cambridge University Press, p.157

Meegan C., Bhat N., Connaughton V., et al., 2007, In: Ritz S., Michelson P., Meegan C.A. (eds.) The First GLAST Symposium. AIP Conf. Ser. 921, p.13

Mitsuda K., Inoue H., Koyama K., et al., 1984, PASJ36, 741

Noble M.S., Nowak M.A., 2008, PASP 120, 821

Nowak M.A., Hanke M., Trowbridge S.N., et al., 2011, ApJ 728, 13

Nowak M.A., Vaughan B.A., Wilms J., et al., 1999, ApJ 510, 874

Pooley G.G., Fender R.P., Brocksopp C., 1999, MNRAS 302, L1

Pottschmidt K., Wilms J., Nowak M.A., et al., 2000, A&A 357, L17

Pottschmidt K., Wilms J., Nowak M.A., et al., 2003, A&A 407, 1039

Poutanen J., Zdziarski A.A., Ibragimov A., 2008, MNRAS 389, 1427

Reid M.J., McClintock J.E., Narayan R., et al., 2011, ApJ 742, 83

Remillard R.A., 2005, In: Chen P. (ed.) Texas@Stanford 2004. SLAC Electronic Conference Proceedings Archive, astro-ph/0504129

Rothschild R.E., Blanco P.R., Gruber D.E., et al., 1998, ApJ 496, 538

Stirling A.M., Spencer R.E., de la Force C.J., et al., 2001, MNRAS327, 1273

von Kienlin A., Meegan C.A., Lichti G.G., et al., 2004, In: Hasinger G., Turner M.J.L. (eds.) UV and Gamma-Ray Space Telescope Systems. SPIE Conf. Ser. 5488, p.763

Vrtilek S.D., Boroson B.S., 2013, MNRAS 428, 3693

Wilms J., Allen A., McCray R., 2000, ApJ 542, 914

Wilms J., Nowak M.A., Pottschmidt K., et al., 2006, A&A 447, 245

Wilms J., Pottschmidt K., Pooley G.G., et al., 2007, ApJ 663, L97

Wilson-Hodge C.A., Case G.L., Cherry M.L., et al., 2012, ApJS 201, 33

Wilson-Hodge C.A., Cherry M.L., Case G.L., et al., 2011, ApJ 727, L40

Xiang J., Lee J.C., Nowak M.A., Wilms J., 2011, ApJ 738, 78

Zdziarski A.A., Pooley G.G., Skinner G.K., 2011, MNRAS 36

Zdziarski A.A., Poutanen J., Paciesas W.S., Wen L., 2002, ApJ 578, 357